the integral is over the thickness L of the plate or lithosphere, and σ is negative under compression [S. P. Timoshenko and J. N. Goodier, *Theory of Elasticity* (McGraw-Hill, New York, ed. 3, 1970), pp. 433–436]. The thermal stress at the surface $z = 0$ is then given by

$$\sigma(t) = -\alpha T_1 E/[3(1-\nu)]$$
$$\{1 - [1 - \exp(-\lambda^2)]/(\lambda\pi^{0.5}) - \mathrm{erfc}(\lambda)\} \quad (2)$$

where $\lambda = L/(4\kappa t)^{0.5}$. For a surface temperature described by a series of step functions, the thermal stress is given by a summation of expressions similar to that above with appropriate shifts in the time since each step change. For the calculations in this report, the surface temperature variation was approximated by step changes spaced 1 My apart in time, and we assumed that $\alpha = 3 \times 10^{-5}$ K^{-1}, $E = 100$ GPa, $\nu = 0.25$, $L = 100$ km, and $\kappa = 1$ mm^2 s^{-1}.

25. R. A. Schultz, *J. Geophys. Res.* **98**, 10883 (1993).
26. M. A. Kreslavsky and A. T. Basilevsky, *ibid.* **103**, 11103 (1998).
27. G. L. Hashimoto and Y. Abe, *Lunar Planet. Sci.* **30**, 1867 (1999).
28. Outgassing twice as much SO_2 and H_2O as in the model of Fig. 2 would result first in the formation of massive sulfuric acid–water clouds that initially cool the surface by 30 to 40 K in the first 150 My (*11*). Subsequent loss of the larger atmospheric inventories of SO_2 and H_2O results in surface temperature excursions that are larger than but qualitatively similar to those in Fig. 2. Warming by about 100 K occurs between 150 and 350 My after the start of the model, and a cooling roughly analogous to that shown at 450 My in Fig. 2 occurs instead at 600 My for the larger eruption. Outgassing half as much SO_2 and H_2O as in the model of Fig. 2 results in temperature excursions that are slightly smaller in magnitude (the early warming is by 45 K instead of 60 K). The rapid loss of clouds and subsequent cooling occurs about 100 My sooner than in Fig. 2.
29. D. L. Turcotte, *J. Geophys. Res.* **88**, A585 (1983).
30. R. J. Phillips and V. L. Hansen, *Science* **279**, 1492 (1997).

31. We thank A. Dombard and R. Phillips for helpful comments. Supported by NASA's Planetary Geology and Geophysics (NAG5-4077) and Planetary Atmospheres (NGW-4982) programs.

15 June 1999; accepted 6 August 1999

The Age of the Carbonates in Martian Meteorite ALH84001

Lars E. Borg,[1]*† James N. Connelly,[2] Larry E. Nyquist,[1] Chi-Y. Shih,[3] Henry Wiesmann, Young Reese[3]

The age of secondary carbonate mineralization in the martian meteorite ALH84001 was determined to be 3.90 ± 0.04 billion years by rubidium-strontium (Rb-Sr) dating and 4.04 ± 0.10 billion years by lead-lead (Pb-Pb) dating. The Rb-Sr and Pb-Pb isochrons are defined by leachates of a mixture of high-graded carbonate (visually estimated as ~5 percent), whitlockite (trace), and orthopyroxene (~95 percent). The carbonate formation age is contemporaneous with a period in martian history when the surface is thought to have had flowing water, but also was undergoing heavy bombardment by meteorites. Therefore, this age does not distinguish between aqueous and impact origins for the carbonates.

The isotopic dating of martian meteorites suggests that differentiation of the martian crust from the mantle occurred no later than 4.53×10^9 years ago (Ga) and was probably contemporaneous with the last stages of planetary accretion (*1*, *2*). It also indicates that there was igneous activity on Mars ~4.5 Ga (*3*, *4*), ~1.3 Ga (*5*, *6*), and as recently as ~200 million years ago (*7*), and suggests that Mars may be geologically active at present. However, little is known about the timing of alteration processes occurring on the martian surface because of the small amount of secondary alteration products in most martian meteorites. In contrast to other martian meteorites, ALH84001 has a substantial amount of secondary carbonate mineralization. Dating of this carbonate can provide insights into surficial processes controlling carbonate formation and cation mobility.

From Sm-Nd analyses, the age of crystallization of ALH84001 was interpreted to be 4.50 ± 0.13 Ga (*3*). The carbonates in ALH84001 were interpreted to be substantially younger at 1.39 ± 0.10 Ga, on the basis of Rb-Sr analysis of shock-melted feldspathic glass and carbonate, and the assumption that these two phases are in isotopic equilibrium (*8*). Equilibrium between feldspathic glass and carbonate is supported by textural observations that the carbonates selectively replace the glass (*9*, *10*). However, the carbonates are Fe- and Mg- rich (*9*–*12*), so that most of their major cations must be derived from a source other than feldspathic glass (Fig. 1). As a result, isotopic equilibrium between carbonate and glass is not assured. Here, we use the results of Rb-Sr and Pb-Pb isotopic analyses on numerous carbonate-rich leachates to determine the age of carbonate formation.

The modal mineralogy of ALH84001 is ~90% orthopyroxene, 2% chromite, ~2% shock-produced feldspathic-glass, ~1% carbonates, and trace amounts of whitlockite, augite, olivine, and pyrite (*9*–*13*). The carbonates form globules and veins along fractures in the meteorite. Compositional zoning from Ca-rich centers, to Fe-rich mantles, to Mg-rich rims is observed in most carbonate occurrences (*9*–*12*). The large chemical variations observed in the carbonates, combined with similar zoning patterns in all occurrences, suggest that they may be products of precipitation in a nearly closed system (*13*–*15*). Thus, carbonates of different composition may be in isotopic equilibrium and be suitable for isotopic dating.

A 1-g chip of ALH84001,170 was crushed and sieved at 150-μm-diameter particles. Composite grains containing carbonate minerals were handpicked, yielding a mineral separate that was ~95% orthopyroxene and ~5% carbonate (determined by visual inspection). There was no visible feldspathic-glass, a potential host for Sr and Pb, in this mineral separate. The high-graded fraction was ultrasonically agitated in quartz-distilled water to remove surface contamination and then leached in a series of progressively stronger reagents (Fig. 1). The leaching procedure was developed from experiments conducted on mixtures of terrestrial calcite, magnesite, siderite, and synthetic whitlockite (supplementary fig. 1) (*16*). The goal of the leaching procedure was to (i) separate soluble carbonates from less soluble silicates; (ii) separate the most easily soluble igneous components, such as whitlockite, from secondary carbonate components; and (iii) separate carbonate components of various compositions.

Uranium-Pb and Rb-Sr were separated sequentially from the leachate fractions by standard cation chromatographic techniques and analyzed by thermal ionization mass spectrometry (Table 1). Laboratory Rb, Sr, and Pb procedural blanks were measured on samples of leaching reagents and applied to individual leachates (*17*). Small (~1% by volume) splits from each leachate were analyzed for Ca, Mg, Fe (by isotope dilution), and P (by colorimetry) to assess contributions of carbonate, phosphates, and silicates to individual leachates (Fig. 1, supplementary fig. 1, and Table 2). Most of the bulk compositions of the leachates (S4 to S8) fall within the range of carbonate analyses (Fig. 1), consistent with a large contribution of carbonate in the leachates. Agreement between the proportions of Ca, Fe, Mg, and P dissolved from the terrestrial carbonates and the proportions of these elements dissolved from the ALH84001 carbonates (supplementary fig. 1) also suggest that the major phase contributing to the leachates is carbonate.

[1]SN2/NASA Johnson Space Center Houston, TX 77058, USA. [2]Department of Geological Sciences, University of Texas at Austin, TX 78713, USA. [3]Lockheed Engineering and Science, 2400 NASA Road 1, Houston, TX 77258, USA.

*Present address: Institute of Meteoritics, University of New Mexico, Albuquerque, NM 87131, USA.

†To whom correspondence should be addressed. E-mail: lborg@unm.edu

About 7.5 mg of carbonate would have to be dissolved to account for the Ca, Mg, and Fe abundances observed in the leachates (Table 2). This is ~3% of the mass of the high-graded fraction, a value that is slightly less than the ~5% carbonate that was estimated to be in the high-graded fraction by visual inspection. Furthermore, the initial 1-g chip of ALH84001 from which the carbonate was separated is expected to yield about 10 mg of carbonate, given reported estimates of ~1% carbonate in the meteorite (*13*). Thus, the abundances of Ca, Fe, and Mg in the leachates are consistent with dissolution primarily of carbonates.

As the strength of the leaching acid increases, the amount of silicate dissolution is expected to increase. Nevertheless, the leaching experiments conducted on terrestrial carbonates demonstrate that ~60% by volume of the siderite was dissolved in the S6 step and that ~55% of the magnesite was dissolved in the S7 step (supplementary fig. 1). In addition, carbonate was observed in a control sample of ALH84001 carbonates and silicates before the S6 leaching step (supplementary fig. 2). Thus, there is experimental and observational evidence that the carbonates contributed to the S6 and S7 leaching steps. Although most of the material dissolved in the leachates is carbonate, the contributions of Rb, Sr, and Pb from other sources, such as terrestrial contamination, phosphates, and silicates, must be assessed for each individual leachate.

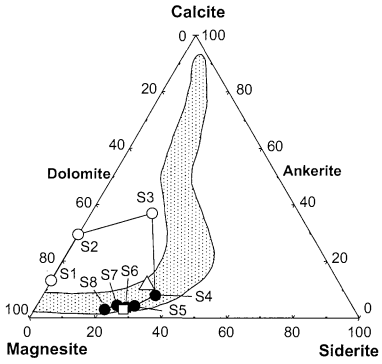

Fig. 1. Ternary diagram illustrating the Ca, Fe, and Mg proportions of the ALH84001 leachates (S1 to S8), assuming carbonate stoichiometry. Stippled area is the range of carbonate compositions determined by (*11*). Open triangle is the bulk carbonate composition, and the open square is the composition of orthopyroxene determined by (*12*). The S1 to S3 leachates do not fall in the field of ALH84001 carbonate microprobe analyses, suggesting that they contain an Fe-poor weathering component such as hydrated magnesite. The S4 to S8 leachates have cation proportions falling within the carbonate field and become progressively more Mg-rich with increasing strength of leaching reagent. The leaching procedure is as follows: S1 (0.01 N acetic acid, 30 min, 23°C), S2 (0.1 N acetic acid, 30 min, 23°C), S3 (0.1 N HCl, 10 min, 23°C), S4 (0.5 N HCl, 15 min, 45°C), S5 (1 N HCl, 15 min, 45°C), S6 (4 N HCl, 20 min, 65°C), S7 (4 N HCl, 40 min, 65°C), and S8 (8 N HCl, 10 min, 65°C).

The leachates become progressively more Mg-rich with increasing acidity of the leaching reagent, as expected from the experiments with terrestrial carbonates in which progressive dissolution of calcite, then siderite, and then magnesite was observed (Fig. 1 and supplementary fig. 1). However, the initial three leachates (S1 to S3) have compositions that do not match carbonate compositions determined by electron microprobe (*11*). Leachates S1 and S2 contained no Fe or P (Table 2) and lie on the magnesite-calcite join (Fig. 1). The corresponding leaching agents were weak (0.01 to 0.1 N acetic acid) and probably removed mainly surface coatings and weathering products, such as hydrated magnesite, that were not removed in the initial water wash. As a result, the S1 to S3 leachates are not used to define the age of the carbonates in ALH84001.

Phosphorous abundances in the S3 and S4 leachates indicate that they contain ~0.16 mg of dissolved whitlockite: ~0.09 mg in the S3 leachate and ~0.07 mg in the S4 leachate. Therefore, whitlockite may contribute to the isotopic systematics of the S4 leachate despite the fact that this leachate has a major element composition that is similar to the bulk carbonate composition estimated by (*12*). A minimal whitlockite contribution is suggested by the observation that the leachates have low abundances of Nd (Table 2) even though Nd abundances in ALH84001 phosphates range from 150 to 209 parts per million (*18*). Mass balance calculations suggest that ~6% of the Sr in the S4 leachate is derived from whitlockite, assuming 100 ppm Sr in whitlockite. Although Pb abundances in martian phosphates are not known, unreasonably high concentrations of 1 ppm would result in ~5% of the Pb in the S4 leachate being derived from phosphates. It is therefore unlikely that phosphates contribute appreciably to the Sr or Pb isotopic systematics of the S4 leachate. The S5 to S8 leachates have no measurable P, indicating that their isotopic systematics are not effected by phosphates.

The low abundances of Rb, Sr, and Pb in mafic silicates preclude substantial contributions of orthopyroxene or olivine to the isotopic systematics of the leachates. For example, the Sr abundance in an orthopyroxene fraction (Px-1R; Fig. 2) was determined to be ~1 ppm. Thus, orthopyroxene could account for a maximum of ~30% of the Sr in the S6 and S7 leachates, assuming that all of the Ca, Fe, and Mg in these leachates is derived from pyroxene. Dissolution of this much pyroxene in the S6 and S7 leaching steps is unreasonable, given that the experiments on terrestrial carbonates demonstrate that the bulk of the carbonate (~60% of the siderite and ~55% of the magnesite) is dissolved in these two leaching steps (supplementary fig. 1) and therefore dominates the Fe and Mg budget of the leachates.

Feldspathic glass has higher Sr and Pb abundances than orthopyroxene or olivine, so that dissolution of small amounts of glass has a greater potential to alter the isotopic systematics of the leachates. However, feldspathic glass was not observed in the high-graded mineral fraction, so that a minimal contribution from this component is expected. This expectation is supported because the leachates that are most likely to dissolve silicates (S6 to S8) tend to have low relative abundances of elements that are enriched in the feldspathic glass, such as Ca, Sr, and K (Table 2).

The calculated Rb-Sr age of the carbonates is relatively insensitive to the leachates chosen to define the isochron (Fig. 2), as long as they have major-cation compositions within the carbonate field (Fig. 1). The calculated age range for two (S4, S5: 3.89 ± 0.05 Ga; S5, S6: 3.93 ± 0.02 Ga), three (S4 to S6: 3.90 ± 0.04 Ga), four (S4 to S7: 3.93 ± 0.04 Ga), or five (S4 to S8: 3.94 ± 0.04 Ga) data points is 3.89 to 3.94 Ga. Our preferred Rb-Sr age of 3.90 ± 0.04 Ga is that determined by the S4 to S6 leachates. This isochron has the chrons considered above. We also prefer the age defined by the S4 to S6 leachates because the isochron is defined by leachates of intermediate strength that are therefore least likely to contain either sur-

Table 1. Isotopic analyses of ALH84001 leachates. S4 to S8 Rb-Sr analyses are weighted averages of two independent runs. Error estimates refer to last digits.

	$^{87}Rb/^{86}Sr$*	$^{87}Sr/^{86}Sr$*†‡	$^{238}U/^{204}Pb$	$^{206}Pb/^{204}Pb$‡§	$^{207}Pb/^{204}Pb$‡§
S1	0.2600 ± 13	0.728746 ± 18	6.353 ± 32	19.356 ± 39	15.994 ± 32
S2	0.2096 ± 11	0.716338 ± 10	43.58 ± 22	20.974 ± 41	16.765 ± 33
S3	0.238 ± 12	0.710308 ± 16	18.80 ± 9	28.934 ± 57	20.277 ± 40
S4	0.1172 ± 12	0.708653 ± 11	21.48 ± 11	36.882 ± 73	23.965 ± 48
S5	0.2327 ± 11	0.715125 ± 10	23.79 ± 12	31.202 ± 61	21.383 ± 43
S6	2.622 ± 13	0.850478 ± 42	40.65 ± 20	27.738 ± 55	20.007 ± 40
S7	2.391 ± 11	0.840711 ± 42	38.26 ± 19	43.211 ± 82	26.736 ± 52
S8	1.421 ± 60	0.787570 ± 18	9.099 ± 45	25.687 ± 49	19.220 ± 37

*Errors limits include minimum uncertainty of 0.5% plus 50% of the blank correction for Rb and Sr added quadratically. †Normalized to $^{86}Sr/^{88}Sr$ = 0.1194. ‡Uncertainties are $2\sigma_m$ calculated from the measured isotopic ratios. §Fractionation correction for Pb is 0.1% per atomic mass unit. Corrected for 9 pg of laboratory blank with $^{206}Pb/^{204}Pb$ = 18.30 and $^{207}Pb/^{204}Pb$ = 15.55.

face contaminants or dissolved silicates.

Several of the leachates (S6 to S8) have high $^{87}Rb/^{86}Sr$ ratios (Table 1 and Fig. 2). The $^{87}Rb/^{86}Sr$ ratios measured in the leachates are higher than the $^{87}Rb/^{86}Sr$ ratios measured in any silicate mineral fractions by (*3*) or the hand-picked, leached Px-1R fraction that was recently analyzed to verify the earlier pyroxene analyses and provide a direct comparison to the carbonate data (Fig. 2). It is therefore unlikely that the elevated $^{87}Rb/^{86}Sr$ ratios reflect dissolution of either pyroxene or feldspathic glass. The high $^{87}Rb/^{86}Sr$ ratios in the S6 to S8 leachates are due to low Sr concentrations in these leachates and not to high Rb concentrations (Table 2) because Rb abundances decrease by a factor of about 10 from the S1 through S8 leachates, whereas the Sr abundances decrease by a factor of about 50.

The Sr concentrations in the carbonate fractions calculated with the S4 to S8 leachates range from 3 to 65 ppm and agree with Sr concentration data measured on the bulk carbonates, which range from 23 to 85 ppm (*19*). A general correlation between Sr and Ca abundances in the leachates suggests that the low Sr in the S6 to S8 leachates may reflect smaller contributions from Ca carbonates in the later leaching steps. The Rb concentrations in the carbonate fractions, calculated with the S6 to S8 leachates, range from 1 to 6 ppm and are lower than in most of the previous leachates characterized by lower $^{87}Rb/^{86}Sr$ ratios.

One potential problem affecting the Rb-Sr age is the possibility of differential leaching leading to laboratory-induced fractionation of Rb and Sr. Fortunately, the Pb-Pb ages of the carbonates are unaffected by parent-daughter fractionation during leaching. The Pb-Pb data define a near-linear array on a $^{207}Pb/^{204}Pb$-$^{206}Pb/^{204}Pb$ isochron (Fig. 3). If all of the leachate data are considered, an age of 4.08 ± 0.06 Ga is defined. However, the S1 to S3 leachates have compositions that are unlike those of the carbonates, fall off the Rb-Sr isochron, and are excluded from the Pb-Pb isochron on this basis. The S8 leachate contains only 40 pg of Pb and is particularly susceptible to laboratory Pb contamination. An age of 4.04 ± 0.10 Ga is defined by the S4 to S7 leachates and has a MSWD of 59. If the S5 leachate is excluded, a more precise Pb-Pb age of 4.03 ± 0.06 Ga (MSWD of 2.2) is defined by the S4, S6, and S7 leachates.

Although the isochron defined by the S4, S6, and S7 leachates has a lower error and MSWD than the age defined by the S4 to S7 leachates, there is no physical reason to exclude the S5 leachate. The Pb abundance in this leachate is about the same as that of the S6 leachate and higher than the S7 leachate, so that laboratory contamination is unlikely to produce the deviation from the isochron. Thus, the S5 leachate is included in the regression to obtain our preferred Pb-Pb age of the carbonates of 4.04 ± 0.10 Ga.

It is apparent that the S1 to S3 leachates fall toward the terrestrial Pb composition defined by modern ocean sediments (*20*) and to the right of the isochrons defined by the remaining samples. It is possible that these fractions contain a component of terrestrial Pb. Terrestrial Pb contamination could have occurred during residence of the meteorite in Antarctica or during sample preparation and chemical separation in the laboratory. Low laboratory procedural blanks of 6 to 11 pg suggest that the terrestrial Pb observed in the S1 to S3 leachates is derived from residence in Antarctica. Lugmair and Galer (*21*) have argued that Pb contamination observed in Antarctic meteorite LEW86010 has an isotopic composition that is similar to that of modern ocean sediments, which in turn is similar to the value used for the laboratory blank composition (Fig. 3 and Table 1). It is therefore not possible to distinguish between contamination in the laboratory and in Antarctica on the basis of Pb isotopic composition. Nevertheless, the presence of Antarctic

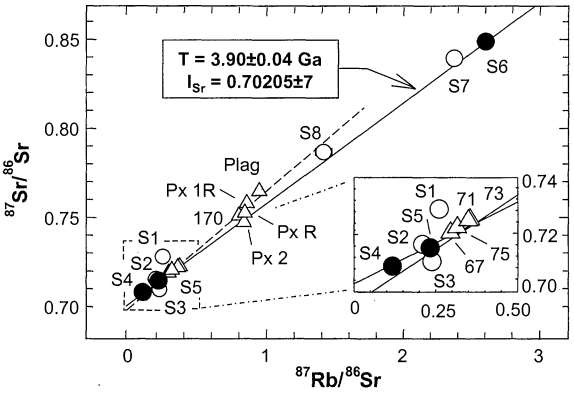

Fig. 2. A Rb-Sr isochron diagram of mineral fractions and whole rocks (open triangles) from (*3*) and the S1 to S8 leachates (circles). Age calculations use a decay constant of 1.402×10^{-11} year^{-1}. An age of 3.90 ± 0.04 Ga (MSWD = 0.67) is defined by the S4 to S6 leachates (solid line; filled circles) with an initial $^{87}Sr/^{86}Sr$ ratio of 0.70205 ± 0.00007 with the program of (*33*). The MSWD is analogous to a chi-squared statistic and indicates the probability that analytical uncertainty will cause the observed amount of scatter of the data about the isochron. The S4 leachate lies on our preferred isochron, suggesting that the whitlockite contribution to its Rb-Sr systematics was small. Those leachates having compositions unlike those of the carbonates (S1 and S2), a high P/Sr ratio (S3), or a very low abundance of Sr (S8) are not collinear with the S4 to S6 leachates. The S7 and S8 leachates appear to lie on a mixing line between the S6 leachate and the previous pyroxene analyses (*3*), suggesting that they may contain a contribution from pyroxene leached by the strong reagents used. On the other hand, these deviations may simply reflect analytical uncertainties associated with analyzing very small amounts of Rb (0.3 to 7 ng) and Sr (0.7 to 9 ng). The S7 leachate has high abundances of major elements and probably contains a large contribution from the carbonate. An age of 3.93 ± 0.04 Ga (MSWD = 4.3) is defined by the S4 to S7 leachates, and an age of 3.94 ± 0.04 Ga (MSWD = 5.8) is defined by the S4 to S8 leachates. The silicate mineral and glass analyses fall near a 4.5-Ga reference line (dashed) defined by the Sm-Nd age (*3*), and the whole rocks lie near the S4 to S6 isochron (**inset**).

Table 2. Cation analyses of ALH84001 leachates. All analyses were determined by isotope dilution with the exception of P, which was analyzed by colorimetry. Cation abundances are in moles (m). One μm = 10^{-6} m, 1 nm = 10^{-9} m, 1 pm = 10^{-12} m, 1 ppm = 10^{-6} g/g, 1 ppb = 10^{-9} g/g.

	wt.* (mg)	Ca† (μm)	Fe (μm)	Mg (μm)	P (μm)	K (nm)	Rb (pm)	Sr (pm)	Nd (pm)	Pb (pm)	K‡ (ppm)	Rb (ppm)	Sr (ppm)	Pb (ppb)
S1	0.16	0.28	0.00	1.58	0.00	25	28	298	1.3	0.42	6071	14.7	163	543
S2	0.20	0.72	0.00	1.49	0.00	24	46	618	12.4	0.66	4817	19.6	271	690
S3	0.29	1.51	0.70	1.68	0.56	28	38	448	210	5.26	3759	11.1	135	3761
S4	1.92	1.80	6.99	11.9	0.50	24	59	1420	69.1	6.68	488	2.62	64.8	723
S5	0.55	0.27	1.72	3.84	0.00	10	21	251	3.8	0.80	732	3.20	40.0	301
S6	1.92	0.84	5.58	14.0	0.00	62	144	155	5.9	0.97	1270	6.40	7.08	105
S7	2.24	1.19	5.82	17.1	0.00	38	82	98	4.6	0.58	671	3.14	3.84	54
S8	0.23	0.08	0.52	1.88	0.00	4	4	8	0.5	0.20	689	1.32	3.11	178
Σ§	7.51	6.69	21.3	53.5	1.06	215	422	3287	307	15.6	1123	4.8	38	430

*Weight of carbonate (1 mg = 10^{-3} g) estimated by using Ca, Fe, and Mg abundances and assuming carbonate stoichiometry. †Adjusted for whitlockite contribution by using P abundances. ‡Concentrations estimated by using estimated weight of carbonate. §Sums of absolute quantities and mass-weighted averages for concentrations.

Pb in the S1 to S3 leachates is not unexpected, given the relative weakness of these leaching reagents and the Pb contamination measured in some Antarctic meteorites (*21*).

The near-linear variation in Pb isotopic compositions of the leachates is probably not the result of mixing between an Antarctic contaminant and phases leached from the meteorite. Although the U-Pb system is disturbed, there is a general positive correlation between U/Pb ratios and Pb isotopic compositions of the leachates (Table 1). This positive correlation suggests that old components, with varying U/Pb ratios and Pb isotopic compositions, were leached from the rock. Multicomponent mixing between meteoritic components with variable Pb isotopic compositions and a terrestrial contaminant added in Antarctica may not be linear unless (i) the composition of terrestrial Pb lies on the Pb-Pb isochron, or (ii) the amount of terrestrial contamination varies proportionally with the Pb isotopic composition of the meteoritic component in the individual leachates. In the first case, the age defined by the Pb-Pb isochron would be unaffected by the addition of Antarctic Pb. The second case is unlikely, given the linearity of the S4 to S7 Pb isotopic data. Concordant, although at the limits of analytical uncertainty, Rb-Sr (3.90 ± 0.04 Ga) and Pb-Pb (4.04 ± 0.10 Ga) ages also suggest that the Pb data define an isochron and not a mixing line.

The estimated age of the carbonates is 500 to 600 million years younger than the 4.50 ± 0.13 Ga age of silicate crystallization (*3*). The resolved difference between the age of silicate crystallization and carbonate precipitation is consistent with formation of the carbonate by an alteration process. The initial $^{87}Sr/^{86}Sr$ ratio of the carbonates is 0.70205 ± 0.00007 (Fig. 3) and requires growth in a reservoir with a $^{87}Rb/^{86}Sr$ ratio of 0.35 from 4.56 to 3.94 Ga. This $^{87}Rb/^{86}Sr$ ratio is about double the $^{87}Rb/^{86}Sr$ ratio of 0.16 estimated for bulk Mars (*1*). Thus, the initial $^{87}Sr/^{86}Sr$ of the carbonates is consistent with a crustal, rather than a mantle, source region. The $^{87}Rb/^{86}Sr$ ratio corresponding to the initial $^{87}Sr/^{86}Sr$ ratio of the carbonates is similar to the $^{87}Rb/^{86}Sr$ ratio measured for the basaltic martian meteorites Shergotty and Zagami, which are thought to have assimilated crustal material to dominate their Rb-Sr systematics (*1*). However, the $^{87}Rb/^{86}Sr$ ratio of 0.35 is greater than the measured $^{87}Rb/^{86}Sr$ ratio for the lherzolitic martian meteorites, which are mantle-derived rocks. Furthermore, the initial $^{87}Sr/^{86}Sr$ ratio of the carbonates appears to be similar to that of the host rock at ~3.9 Ga because the whole-rock points fall on or near the carbonate isochron (Fig. 2). This suggests that the carbonates formed from a source that was isotopically similar to the silicate host rock and are therefore of probable local derivation. Models of carbonate formation that require the import of cations from large distances are less probable because the fluids involved would not be expected to have the same $^{87}Sr/^{86}Sr$ ratio as the host rock.

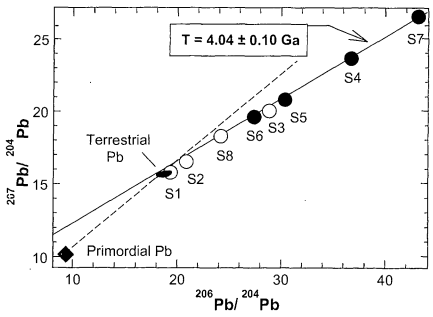

Fig. 3. A Pb-Pb isochron plot of the ALH84001 leachates (circles). An age of 4.08 ± 0.06 Ga (MSWD = 279) is defined by all of the leachates, an age of 4.04 ± 0.10 (MSWD = 59) is defined by the S4 to S7 leachates (solid line; filled circles), and an age of 4.03 ± 0.06 Ga (MSWD = 2.2) is defined by the S4, S6, and S7 leachates. A 4.5-Ga reference line (dashed) passes through the primordial Pb value of (*34*). Terrestrial Pb (filled oval) is represented by marine sediments (*20*) and best reflects the Pb composition of Antarctic contamination (*21*). Addition of Antarctic contamination probably causes the S1 to S3 leachates to fall off this isochron. Low Pb abundances in S8 make this leachate particularly susceptible to contamination in the laboratory.

During the period in which the carbonates formed, Mars is argued to have been wetter and warmer than at present (*22–24*). At the same time Mars may have undergone heavy bombardment by meteorites [for example, (*25*, *26*)]. Thus, the old age of the carbonates is consistent with models of carbonate formation by precipitation from fluids at low temperature (*13*, *27*, *28*), as well as with models in which carbonates are produced by impact-driven metasomatism (*11*) or impact melting of preexisting carbonates (*14*, *29*).

The Ar-Ar ages determined on ALH84001 whole rocks are within error of the Rb-Sr and Pb-Pb ages of the carbonates. The Ar-Ar ages have been interpreted to range from 3.8 to 4.3 Ga (*30*, *31*) and reflect the time of Ar outgassing by impact metamorphism. Concordance between the Ar-Ar age of ALH84001 and the Rb-Sr and Pb-Pb age of the carbonates is consistent with the suggestion that the carbonates could have been produced by impact processes (*11*, *14*, *29*). However, there is a significant amount of time represented by the analytical uncertainties of the various ages. Thus, the carbonate formation age and the age of the impact event might be analytically indistinguishable and yet be separated by tens to hundreds of millions of years.

A direct causal relationship between impact and carbonate formation is consistent with a high-temperature origin of the carbonates and would not support the hypothesis of (*32*) that relicts of ancient martian life are preserved in the carbonates of ALH84001. However, carbonate precipitation at low temperature might be indirectly impact-related. For example, an impact could shock the host rock, resetting the Ar-Ar age, melt surficial ice, and/or create a basin that collects water for the precipitation of the carbonates. In this scenario, the carbonates would be deposited in a single event, as required by isotopic equilibrium between the various leachates. This event must be relatively short-lived, as suggested by the absence of secondary hydrous phases observed in ALH84001 (*14*, *28*). Impact release of water from the frozen subsurface could also facilitate rock and water interactions producing a fluid that contained high concentrations of Ca, Fe, and Mg with which to form the carbonates. The agreement between the Sr isotopic systematics of the carbonate and silicate phases places some constraints on the source of the carbonate cations. The fluids could have equilibrated with either local surface rocks isotopically similar to ALH84001 or with surface rocks that are isotopically homogeneous over a large portion of the martian surface.

References and Notes

1. L. E. Borg, L. E. Nyquist, L. A. Taylor, H. Wiesmann, C.-Y. Shih, *Geochim. Cosmochim. Acta* **61**, 4915 (1997).
2. C. L. Harper, L. E. Nyquist, B. M. Bansal, H. Wiesmann, C.-Y. Shih, *Science* **267**, 213 (1995).
3. L. E. Nyquist, B. M. Bansal, H. Wiesmann, C.-Y. Shih, *Lunar Planet. Sci. Conf.* **26**, 1065 (1995).
4. E. Jagoutz, *Meteoritics* **29**, 478 (1994).
5. C.-Y. Shih, L. E. Nyquist, H. Wiesmann *Lunar Planet. Sci. Conf.* **27**, 1197 (1996).
6. N. Nakamura, D. M. Unruh, M. Tatsumoto, R. Hutchison, *Geochim. Cosmochim. Acta* **46**, 1555 (1982).
7. C.-Y. Shih *et al.*, *ibid.*, p. 2323.
8. M. Wadhwa and G. W. Lugmair, *Meteoritics* **31**, A145 (1996).
9. A. H. Trieman, *ibid.* **30**, 294 (1995).
10. J. D. Gleason, D. A. Kring, D. H. Hill, W. V. Boynton, *Geochim. Cosmochim. Acta* **61**, 3503 (1997).
11. R. P. Harvey and H. Y. McSween Jr., *Nature* **382**, 49 (1996).
12. D. W. Mittlefehldt, *Meteoritics* **29**, 214 (1994).
13. C. S. Romanek *et al.*, *Nature* **372**, 655 (1994).
14. E. R. D. Scott, A. Yamaguchi, A. N. Krot, *ibid.* **387**, 377 (1997).
15. G. A. McKay and G. E. Lofgren, *Lunar Planet. Sci. Conf.* **28**, 921 (1997).
16. Supplemental web material is available at www.sciencemag.org/feature/data/ 1044621.shl.
17. Rb blanks ranged from 3 to 11 pg and contributed <0.3% of the Rb to the S1 to S7 leachates and <1% of the Rb to the S8 leachate. Sr blanks ranged from 16 to 35 pg and contributed <0.2% of the Sr measured in the S1 to S7 leachates and 5% of the Sr inthe S8 leachate. The Pb blanks ranged from 6 to 11 pg and contributed from 3 to 16% of the Pb in individual leachates.
18. M. Wadhwa and G. Crozaz, *Meteoritics* **33**, 685 (1998).
19. J. D. Gilmour, J. A. Whitby, G. Turner, *ibid.* **32**, A48 (1997).
20. D. Ben Othman, W. M. White, J. Patchett, *Earth Planet. Sci. Lett.* **94**, 1 (1989).
21. G. W. Lugmair and S. J. G. Galer, *Geochim. Cosmochim. Acta* **56**, 1673 (1997).
22. F. P. Fannale, S. E. Postawko, J. B. Pollacj, M. H. Carr, R. O. Pepin, *Mars*, H. H. Kieffer, B. M. Jakosky, C. W. Snyder, M. S. Matthews, Eds. (Univ. of Arizona Press, Tucson, AZ, 1992), pp. 1135–1179.

23. M. H. Carr, *Icaurus* **56**, 476 (1983).
24. _____ *Water on Mars* (Oxford Univ. Press, xx, 1996), p. 229.
25. W. K. Hartmann *et al.*, *Basaltic Volcanism on the Terrestrial Planets* (Pergamon, New York, 1981), pp. 1049–1127.
26. G. Neukum and D. U. Wise, *Science*, **194**, 1381 (1976)
27. H. Y. McSween Jr. and R. P. Harvey, *Int. Geol. Rev.* **40**, 774 (1998).
28. P. H. Warren, *J. Geophys. Res.* **103**, 16759 (1998).
29. E. R. D. Scott, A. N. Krot, A. Yamaguchi, *Meteoritics* **33**, 709 (1998).
30. G. Turner, S. F. Knot, R. D. Ash, J. D. Gilmour, *Geochim. Cosmochim. Acta* **61**, 3835 (1997).
31. D. D. Bogard and D. H. Garrison, *Meteoritics* **34**, 451 (1999).
32. D. S. McKay *et al.*, *Science* **273**, 924 (1996).
33. D. York, *Can. J. Phys.* **44**, 1079 (1966).
34. M. Tatsumoto, R. J. Knight, C. J. Allègre, *Science* **180**, 1279 (1973).

35. We thank K. Manser for assistance with U-Pb analyses and D. C. Golden for assistance with P analyses. We also thank three anonymous reviewers for comments on the manuscript. This work was supported by NASA RTOP numbers 344-35-05-02 and 344-31-00-05 and was completed while L.E.B. held a National Research Council (Johnson Space Center) Research Associateship.

21 June 1999; 17 August 1999

The Gravity Field of Mars: Results from Mars Global Surveyor

David E. Smith,[1]* William L. Sjogren,[2] G. Leonard Tyler,[3] Georges Balmino,[4] Frank G. Lemoine,[1] Alex S. Konopliv[2]

Observations of the gravity field of Mars reveal a planet that has responded differently in its northern and southern hemispheres to major impacts and volcanic processes. The rough, elevated southern hemisphere has a relatively featureless gravitational signature indicating a state of near-isostatic compensation, whereas the smooth, low northern plains display a wider range of gravitational anomalies that indicates a thinner but stronger surface layer than in the south. The northern hemisphere shows evidence for buried impact basins, although none large enough to explain the hemispheric elevation difference. The gravitational potential signature of Tharsis is approximately axisymmetric and contains the Tharsis Montes but not the Olympus Mons or Alba Patera volcanoes. The gravity signature of Valles Marineris extends into Chryse and provides an estimate of material removed by early fluvial activity.

The gravity field of Mars reflects internal and external processes over several billion years, similar to the moon's. However, the magnitude of the variations on Mars indicates stress differences of about six times those in the Moon. The radio science investigation on the Mars Global Surveyor (MGS) mission (*1*) has developed global high-resolution gravitational field models (Fig. 1) for Mars from tracking data (Table 1) (*2, 3*) and provides new insight into the manner in which Mars has evolved through time in response to major impacts, surficial geological processes, and internal dynamics.

Tracking of the Mariner-9 and Viking-1 and -2 orbiters had limited coverage and lower accuracy data (*2, 4–6*) than MGS. The largest free-air gravity anomalies on Mars (Fig. 1A) associated with Olympus Mons and the Tharsis Montes (Ascraeus, Pavonis, and Arsia volcanoes) exceed 3000 mgal (*3*), more than an order of magnitude greater than those on Earth (*9*) for similar wavelengths (*10*). The substantial gravitational power (Fig. 2) is indicative of the ability of the planet's lithosphere to support large stresses associated with surface and subsurface loads (*11*). The thick lithosphere on Mars is a consequence of the more rapid loss of accretional and radiogenic heat from the martian interior as compared with Earth's. A striking feature of the field is the limited range of anomalies (± ~100 mgal) over a large fraction of the planet. Anomalies with substantial amplitudes are limited to the Tharsis, Isidis, and Elysium regions in the eastern and western hemispheres. A broad high of ~100 mgal in the midlatitude eastern hemisphere surrounds the Hellas basin and appears to be associated with material excavated from this structure (*12*).

Mars' gravitational potential, or areoid (*13*) (Fig. 1B), displays two hemispheric-scale quasi-circular features with a dynamic range of more than 2 km, an order of magnitude greater than that observed for Earth. The Tharsis Montes, Olympus Mons, Valles Marineris, and Isidis impact basin are resolved as individual gravitational anomalies in the areoid. Of particular note is the apparent circularity of the Tharsis areoid feature, in contrast to the complex topography of the region (*12*). The central portion of the Tharsis areoid encompasses the three Tharsis Montes in a single large anomaly and isolates Olympus Mons to the northwest. The Alba Patera volcanic construct also appears as a subtle feature separated from the main Tharsis areoid feature. The separation of Olympus and Alba from the main dome of Tharsis is similar to the topographic separation (*12*) and indicates that these prominent volcanic shields have distinctive source regions in the mantle that may explain the topography.

The zonal variation of gravity anomalies (Fig. 3) shows differences between the southern and northern hemispheres: the lack of gravity anomalies below major topographic features over most of the southern hemisphere, as well as substantial anomalies that lack topographic expression in the northern hemisphere. The smooth character of the gravity indicates that the topography in the southern latitudes is isostatically compensated much as are highland terrains on the moon (*14*).

The range of gravity variation from south to north (Fig. 3A) increases to as large as ~160 mgal. This suggests a latitude-dependent variation in compensation that may be associated with Mars' pole-to-pole 0.036° slope in topography (*12*) that might be explained by a systematic variation of crustal thickness with latitude. The longitudinal variation of gravity anomalies between latitudes 20°N to 75°N (Fig. 3B), and 20°S to 75°S (Fig. 3C) also emphasizes the difference between the two hemispheres. The uniform gravity field over most of the southern hemisphere in comparison with the much higher amplitude variation seen in the north is the antithesis of the topography, which is smooth in the north and rugged in the south. This points to a quantitative difference in the evo-

Table 1. Summary of spacecraft tracking data.

Spacecraft	Periapsis height (km)	Inclination (degrees)	Tracking
Mariner 9	1600	64	S-band Doppler
Viking 1	300, 1500	39, 55	S-band Doppler
Viking 2	300, 800, 1500	55, 75, 80	S-band Doppler
MGS	380, 263, 170	93	X-band Doppler, range

[1]Laboratory for Terrestrial Physics, National Aeronautics and Space Administration (NASA) Goddard Space Flight Center, Greenbelt, MD 20771, USA. [2]Jet Propulsion Laboratory, Pasadena, CA 91109, USA. [3]Center for Radio Astronomy, Stanford University, Stanford, CA 94035–4055, USA. [4]Group de Recherches de Geodesie Spatiales, Toulouse, France.

*To whom correspondence should be addressed: dsmith@tharsis.gsfc.nasa.gov